EARTH FEATURE IDENTIFICATION FOR ONBOARD MULTISPECTRAL DATA EDITING: COMPUTATIONAL EXPERIMENTS

R. M. Aherron
Information & Control Systems, Inc.*

R. F. Arduini
Computer Sciences Corporation*

R. E. Davis, F. O. Huck, S. K. Park
NASA Langley Research Center*

ABSTRACT

A computational model of the processes involved in multispectral remote sensing and data classification is being developed as a tool for designing smart sensors which can process, edit and classify the data that they acquire. An evaluation of sensor system performance and design tradeoffs can be expected to involve classification rates and errors as a function of number and location of spectral channels, radiometric sensitivity and calibration accuracy, target discrimination assignments, and accuracy and frequency of compensation for imaging conditions. This model seeks to provide a link between the radiometric and statistical properties of the signals to be classified and the performance characteristics of electro-optical sensors and data processing devices. Preliminary computational results are presented which illustrate the editing performance of several remote sensing approaches.

INTRODUCTION

To overcome present inefficiencies in worldwide monitoring of resources and the environment by remote multispectral sensing, it is necessary to develop multispectral sensor systems which are "smart" enough so that they can be relied upon to perform such tasks as identifying and locating features of interest, editing out areas of extensive cloud cover and haze, and compensating for atmospheric variability. The development of such smart-sensor systems must take into account the complex natural variability of surface and cloud reflectance and atmospheric radiative transfer. To do so, smart-sensor concepts should be developed and evaluated first as models in the computer, and only thereafter, if promising, as actual devices and systems.

A comprehensive computational model of the deterministic and stochastic processes involved in remote sensing is currently being developed as such a tool for studying multispectral sensor systems and concepts.[1] This model accounts for remote multispectral data acquisition and processing as a function of both deterministic and stochastic elements of solar irradiance, atmospheric radiative transfer, surface and cloud reflectance, and sensor response. The model differs from other related efforts[2-7] in two aspects: One, it treats all elements of the remote sensing process as parts of a single system. Two, it specifically relates stochastic properties of the sensor signal to stochastic properties of the atmospheric radiative transfer and scene spectral reflectance.

*Located in Hampton, Virginia.

In this paper we use the computational model of the remote sensing process to study earth feature identification algorithms for onboard data editing. The objective of the feature identification task is to distinguish between vegetation, bare land, water, clouds and snow. If such discrimination between these categories could be made with reasonable accuracy and computational simplicity, then onboard data processing could be relied upon to reduce drastically the amount of data that needs to be transmitted and processed for routine remote sensing operations.

The analysis in this paper is limited to two spectral channels which are centered at wavelengths 0.65 and 0.85 μm. These spectral channels are particularly well-suited for distinguishing vegetation from other earth surface features. For that reason they have been selected for the Feature Identification and Location Experiment (FILE) on Shuttle-OSTA 1. These two channels correspond closely to channels 3 and 4 of the Thematic Mapper (TM) and Multispectral Linear Array (MLA)[8] so that the results presented in this paper are relevant to data processing studies concerned with future remote sensor systems for monitoring earth resources and the environment. Results presented in this paper compare the relative accuracy and computational complexity of three decision techniques for performing the feature identification task. The driving variables are atmospheric conditions, solar incidence angle, and spectral reflectance properties. No attempt is made here to distinguish between clouds and snow since clouds are most efficiently identified, and discriminated from snow and ice, in the reflected IR around 1.5 μm and the emitted IR around 10 to 12 μm (atmospheric window).[9-10]

REMOTE SENSING MODEL

In this section we briefly review the computational remote sensing model developed by Huck et al.[1] The model accounts, as depicted in Fig. 1, for data acquisition and classification. Data acquisition must account for the solar irradiance, atmospheric radiative transfer, surface reflectance, and sensor response. In mathematical terms, data classification is that process that maps the very large sensor sample space into a much smaller space of predefined categories or features. It is essentially the feature identification algorithm that defines these categories.

Radiative Transfer

Deterministic Processes - When atmospheric attenuation (absorption and scattering) and Lambertian ground reflectance effects are taken into account, the radiance derived from solar spectral irradiance incident on a downward-looking sensor is represented as:

$$L = \frac{1}{\pi} E_o \, T_o \, \mu_o \, \rho \, T + L_d \, \rho \, T + L_p \qquad (1)$$

where $E_o \equiv E_o(\lambda)$ is the solar spectral irradiance at the top of the atmosphere; $T_o \equiv T_o(\lambda,\tau,\mu_o)$ is the atmospheric transmittance along the incident path from the sun to the surface (solar zenith angle = θ_o, $\mu_o = \cos\theta_o$); $L_d \equiv L_d(E_o,\lambda,\tau,\mu_o,\rho)$ is the diffuse sky spectral radiance which results from all radiation scattered downward onto the surface (i.e., integrated at the target over elevation and azimuth); $\rho \equiv \rho(\lambda)$ is the spectral reflectance of the surface (sometimes called "signature"); $T \equiv T(\lambda,\tau,\mu)$ is the atmosphere transmittance along the exitant path from the surface to the sensor (zenith angle = θ, $\mu = \cos\theta$); and $L_p \equiv L_p(E_o,\lambda,\tau,\mu_o,\mu,\phi)$ is the path spectral radiance which results from all radiation scattered upward along the path from the surface to the sensor. The other parameters are wavelength, λ, optical thickness of the atmosphere $\tau \equiv \tau(\lambda)$, and azimuth angle ϕ between the planes of incidence and exitance. The component of the total

radiance L which arises from radiation reflected from the target is referred to as the beam spectral radiance L_b, that is, $L_b=L-L_p$ and $L_b \equiv L_b(E_o,\lambda,\tau,\mu_o,\mu,\rho)$.

The optical thickness $\tau \equiv \tau(\lambda)$, which governs atmospheric transmittance, sky and path radiance, is given by

$$\tau = \sum_{i=1}^{N} \alpha_i \, x_i \qquad (2)$$

where $\alpha_i \equiv \alpha_i(\lambda)$ is the attenuation coefficient of the ith atmospheric constituent and x_i the associated attenuator amount (often denoted u_i in the radiative transfer literature). The atmospheric transmittance over the incident path is given by $e^{-\tau/\mu_o}$, and that over the exitant path by $e^{-\tau/\mu}$. The rigorous treatment of multiple scattering which leads to sky and path radiance is very difficult and computationally expensive. To use documented atmospheric radiative transfer models and to keep computations with the deterministic/stochastic model economical, we use the AFGL LOWTRAN 4[11] model to account for attenuation in atmospheric absorption bands and the ERIM model (developed and described by Turner[3-4]) to account for scattering. For the spectral region extending from 0.4 to 1.0 μm, the atmospheric radiative transfer is primarily affected by Rayleigh scattering (by air molecules N_2 and O_2), scattering by aerosols (haze droplets and dust), and absorption by ozone (O_3), water vapor (H_2O), and molecular oxygen (O_2).

The ERIM radiative transfer model is used to account for single and multiple scattering in the atmosphere for a surface with a simple geometric pattern. We assume a horizontally homogeneous atmosphere which is bounded by a surface that consists of an infinitesimally small target and a large surrounding background, both of which have uniform diffuse (Lambertian) reflectances. The model accounts for realistic anisotropic phase functions and vertical changes in the atmosphere and for attenuation by ozone absorption and aerosol and molecular scattering but not for attenuation by water vapor and molecular oxygen. This limitation constrains the application of the ERIM model to the evaluation of spectral responses that do not significantly overlap the major H_2O (0.86 to 0.99 μm) and O_2 (0.75 to 0.77 μm) absorption bands. More comprehensive computational models are available but their use as subroutines would be too expensive.

The difference between the LOWTRAN 4 and ERIM models can be expressed in terms of Equation 1. Both models calculate the first term in the same way. LOWTRAN 4 does not, however, include either the second or the third terms which represent scattered solar radiation.

Stochastic Processes - We regard the spectral radiance $L \equiv L(\lambda)$ that reaches the sensor as a stochastic process whose value at each wavelength depends upon a number of random variables associated with both the atmosphere and surface. Letting the operation $E\{\cdot\}$ denote the expectation (average) taken over the ensemble of all possible radiances associated with a particular surface, the mean $\langle L(\lambda) \rangle$ and autocovariance $C_L(\lambda,\lambda')$ of the radiance can be expressed as

$$\langle L(\lambda) \rangle = E\{L(\lambda)\}$$

and

$$C_L(\lambda,\lambda') = E\{[L(\lambda) - \langle L(\lambda) \rangle][L(\lambda') - \langle L(\lambda') \rangle]\}$$

To simulate the effects of atmospheric variability, we assume that the attenuator amounts x_i in Equation 2 are random variables with a known mean x_i and covariance σ_{ii}.

It is particularly convenient, although not necessary for the purpose of simulation, to assume that the vector of attenuator amounts is multivariate Gaussian. Therefore the optical thickness will have a log-normal distribution.

To simulate the effects of surface reflectance variability, we model the reflectance of a particular target surface by

$$\rho(\lambda) = \rho_o(\lambda)\ e^{-x_o\beta_o(\lambda)}$$

where $\rho_o(\lambda)$ and $\beta_o(\lambda)$ are deterministic functions which are characteristic of the surface, and x_o is a standard normal random variable with mean = 0 and variance = 1. For each surface the parameters $\rho_o(\lambda)$ and $\beta_o(\lambda)$ are estimated from empirical reflectance data.

Signal Vector and Reference Pattern

The sensor converts the radiance L into the signal vector s with components s_j which are represented by the simple model

$$s_j = \int_0^\infty L(\lambda)\ S_j(\lambda)\ d\lambda$$

where $S_j(\lambda)$ is the deterministic spectral response of the jth channel. Effects due to electronic noise and errors in radiometric calibration are not treated here, in order to simplify the following formulations.

Because the radiance is stochastic, the signal vector s is a multivariate random variable whose mean r and covariance C have components denoted by

$$r_j = E\{s_j\}$$

and

$$c_{jj} = E\{(s_j - r_j)(s_{j'} - r_j)\}$$

where both j and j' take on the values 1, 2, ..., J, and J is the total number of channels. It follows from the linearity of the signal conversion process that the reference patterns can be computed as

$$r_j = \int_0^\infty \langle L(\lambda)\rangle\ S_j(\lambda)\ d\lambda$$

and

$$c_{jj} = \int_0^\infty \int_0^\infty C_L(\lambda,\lambda')\ S_j(\lambda)\ S_{j'}(\lambda')\ d\lambda\ d\lambda'$$

RADIOMETRIC PROPERTIES AND SENSOR RESPONSES

In this section we present typical radiometric properties encountered in remote sensing and the spectral responses of the FILE sensor system. Our characterizations here are confined to a spectral region of 0.4 to 1.0 μm.

Model Inputs

Solar irradiance - The solar spectral irradiance $E_o(\lambda)$ incident upon the top of the atmosphere is relatively well known and is shown in Figure 2. Its variability is small compared to other uncertainties and thus is ignored here.

Surface reflectance - Table 1 summarizes the categories and substances used as examples in this investigation as well as the (assumed) standard deviations of their reflectances. The spectral reflectance curves are shown in Figure 3. Typical variability of spectral reflectances realized in the simulation is shown in Figure 4.

Atmospheric properties - The mean whole-atmosphere (i.e., vertical path) attenuator amounts for each of these atmospheric constituents, along with reasonable values of their standard deviations based on estimates of climatological variability, are listed in Table 2. All attenuator amounts are assumed to be uncorrelated, except for water vapor and aerosol which are assumed to have a perfect positive correlation. Figure 5 shows a plot of typical average radiance components. Figure 6 shows a typical realization of simulated radiance variability using the LOWTRAN 4 model.

Sensor response - The FILE system consists of two sensors, one centered at .65 μm and one centered at .85 μm. These are relatively narrow-band sensors spectrally (20 nm bandwidth), compared to the 100 to 300 nm bandwidth used in the LANDSAT sensor system. The sensor bandwidths do not overlap any major atmospheric absorption bands. The FILE system includes an onboard categorizer that assigns each pixel to bare land, vegetation, water, or snow/clouds. The FILE sensor channels were originally chosen because of the desirable properties of the ratio of the two channel outputs. Also, channel ratios have some useful compensation effects for sun angle and atmospheric variability.[12]

FEATURE IDENTIFICATION TECHNIQUES

In this section we describe three methods that could be used to identify (edit) such categories as vegetation, bare land, water, and cloud/snow. Two of these methods are closely related; they use either the maximum likelihood (MLH) or mean-square distance (MSD) classification algorithms to classify the signal vectors according to reference patterns (or training sets) and then collect all classes into categories. The third method, referred to as the boundary approximation method (BAM), avoids the classification step and assigns the signal vectors directly into categories.

Classification

A very common classification procedure which makes use of covariance information is based upon maximizing the (assumed) Gaussian PDF. Specifically, a particular signal vector, s, representing J spectral channels, is classified as spectral type n, provided the Gaussian PDF of s conditioned on spectral type n is largest, i.e., provided

$$\mathrm{PDF}(s|n) = \frac{1}{(2\pi)^{J/2}|C_n|^{1/2}} \exp\left[-\frac{1}{2}(s-r_n)^t C_n^{-1}(s-r_n)\right] \tag{3}$$

is greater than PDF $(s|n')$ for all other spectral types $n' = 1, 2, \ldots N$. To avoid the computational expense of evaluating the exponential, an equivalent classification

procedure can be used which minimizes $-\log_e$ [PDF $(s|n')$]. This, in turn, is equivalent to determining the n which minimizes

$$(s-r_n)^t\ C_n^{-1}\ (s-r_n) + \log_e|C_n| \qquad (4)$$

where $|\cdot|$ denotes determinant. If the a priori probability of each spectral type is known (and all types are not equally likely), it is often desirable to weight the classification procedure by this prior information. However, no weighting is used for the results presented in this paper. For this classifier, the mean and covariance matrix uniquely determine a class. This is the maximum likelihood classifier (MLH).

Several simplifying assumptions concerning the nature of the covariance matrix, given imperfect knowledge, can be made. In the special case of

$$C_n = I$$

where I is the identity matrix, minimizing Equation 4 becomes equivalant to minimizing

$$(s-r_n)^t\ (s-r_n)$$

This is commonly called the mean-square distance (MSD) or Euclidean-distance classifier. From a computational standpoint, we eliminate the evaluation of one vector-matrix (1xn * nxn) multiplication and the addition of the logarithm term. For this special case the mean uniquely determines the class.

Editing

Aggregation method - The MLH and MSD classification algorithms work with classes but can be used to distinguish between categories such as vegetation, bare land, water, and clouds/snow by collecting a set of classes to define each of the four categories. For example, if one can pick some small number of vegetation classes that approximate (span) the vegetation category then one has a method of categorizing vegetation. In other words one can blanket the area, in spectral space, occupied by the vegetation category with a set of classes. Computationally, what can be done is to actually assign a signal to a class (according to the chosen decision rule) but to only retain the category within which that class falls. For example, a signal from a corn target might be classified as wheat but the editor retains only the fact that it has been categorized as vegetation. The overall accuracy of categorizing will be higher than the overall classification accuracy because intra-category class confusion is not counted as wrong. We call this method categorization by aggregation.

Boundary approximation method - In discussing this editing technique frequent reference will be made to covariance ellipse plots. These ellipses are defined by the following equation:

$$(x-r_n)^t\ C_n^{-1}\ (x-r_n) = 1$$

where x is the channel vector. If the nth class was truly multivariate-Gaussian then this ellipse would enclose 66% of the data. The ellipses are centered about the class mean. These plots provide a very useful approximation to the scatter of the data due to such things as the variability in radiance shown in Figure 6. Figure 7 shows ellipse plots for simulated data for a total of twenty classes. This data represents a simulation for 23 km visual range and a solar zenith angle of 30°, using the FILE channels.

As stated previously this particular set of FILE spectral bands was chosen because of the properties that the channel ratio possessed. Figure 7 shows 3 lines superimposed. The lines are chosen so as to delineate the four categories. These lines represent simple approximations to the boundaries of the categories in spectral space. Hence the name Boundary Approximation Method (BAM). The lines drawn are not strictly defined by the channel ratios. It was decided that, by adding an offset to the two diagonal equations, much better performance could be achieved. This causes only a slight increase in computational costs. The third line represents an "absolute" radiance threshold which forms the boundary between the bare land and snow/cloud, categories which have similar channel ratios. However, this threshold has a sensitivity to solar zenith angle.[12] The three boundaries are defined by the following equations. If x_i is the value of channel i then the three lines are defined as:

$$x_2 = 1.45\, x_1 - 4.1$$
$$x_2 = 3.0\, x_1 - 2.1$$
$$x_2 = 16.5$$

As one can see this method is very simple in terms of the calculations necessary to categorize a signal and is similiar to the standard parallelepiped classifiers. This method represents the opposite end of the spectrum, in terms of computational complexity, from the aggregation method.

Space qualified data processing hardware is still rather expensive and bulky. Any implementation of onboard processing of multispectral data will encounter very conservative limits in terms of available processing and storage capacity. This, in turn, limits the computational "costs" that can be incurred in identifying features. Estimates of the computational complexity of the two methods of aggregation were made after the formulas were simplified and modified as much as possible. No provision was made for special processing architecture (i.e., parallelism) in the estimates. For the boundary approximation technique we have two equations to evaluate with 1 add and 1 multiply each for a total of 4 add/multiplies. The number of add/multiplies per pixel necessary to do the MSD classification, and thus editing, can be approximated by 2LJ where L is the number of classes and J is the number of channels. Similarly, the number for PDF can be approximated by $(L/2)(J^2+3J)$. Those interested in more details might start with Ref. 13 and 14.

COMPUTATIONAL EXPERIMENTS AND RESULTS

Experiments

In this section we present results of computational experiments which illustrate the performance of the MLH and MSD aggregation and the boundary approximation methods in distinguishing between such spectral features as vegetation, bare land, water, and cloud/snow from data obtained with the two FILE spectral channels. These two channels are centered at 0.65 and 0.85 μm and thus approximately coincide with TM/MLA sensor channels 3 and 4. The results provide insight into the susceptibility of feature identification accuracy on the natural variability of atmospheric radiative transfer and target and background spectral reflectance.

The computer program (previously described) simulating the performance of an orbiting multispectral sensor generates pseudo-random observations (i.e., signal vectors) which are assembled into training sets for computing a reference pattern library. Subsequently, observations are generated for input to the editor/classifier which utilizes the reference pattern library or other criteria to make its decision.

Editing accuracy (i.e., the ratio of correct categorizations to the total number of observations) is used as a figure of merit to determine sensor performance. Training sets and editing accuracies are based upon a total of 100 observations per target.

In practice, classification using the elements of a reference library will always be compromised since these elements must be based upon values for the means and covariances obtained at one specific set of conditions. For example, the reference library may have been compiled when the atmosphere was relatively clear, while the observations were made when the atmosphere was hazier. This error source has been included by computing the reference vector r and covariance matrix C for each target at a visual range of about 23 km (representing a moderately clear atmosphere), and the signal vectors s either at the same visual range or at reduced visual ranges of about 10 km and 5 km. Similarily, to assess the effect of changes in solar incidence angle, reference data were obtained for a solar incidence angle of 30°, whereas feature identification decisions were made either at the same or at 40° solar incidence angle. The sensor viewing geometry remained vertical.

Results

Figure 8 summarizes the predicted feature identification accuracy, and Table 3 presents the amount of computations required for the three decision processes. The feature identification accuracies are complex functions of changes in task assignment, visual range, and solar incidence angle. Nevertheless, it can be concluded that the MLH and MSD aggregation methods provide consistently higher feature identification accuracies than the BAM and also tend to be less susceptible to changes in both visual range and solar incidence angle. However, this improvement is gained at a substantial increase in computational and storage requirements. These requirements would increase rapidly for the MLH and MSD aggregation methods with increases in the number of substances to be accounted for and in the number of spectral channels to be used. One can also see that for a 3-fold increase in computational cost little or nothing is gained in terms of increased accuracy or sensitivity to sun angle by using the MLH as opposed to the MSD. The results in figure 8 serve to show that small changes in the mix of classes, observed by the sensor, can have as important an effect as the other sources of error, such as atmospheric degradation. Specifically, ripening barely lacks the strong chlorophyll absorption band that the .65 μm channel is designed to detect in vegetation. Therefore, barley is likely to be confused with bare land.

These results suggest that BAM could become a useful algorithm for spectral feature identification if it is expanded to use more than 2 spectral channels and if changes in solar incidence angle could be accounted for. It would, of course, also be desirable to account for changes in visual range; however, this would be more difficult.

In practice the exact formulation of an algorithm depends on the particular task. For example, in editing out clouds, errors of omission, whereby we retain some cloud data, are less troublesome than errors of commission, whereby we edit out data from other categories. In general, if one particular category is of interest the boundaries for that category can be "relaxed" somewhat in order to pick up marginal outliers. In more complete analysis the a priori probabilities of each of the categories are needed in order to optimize the omission-commission trade-offs. This is also true for the aggregation method.

CONCLUDING REMARKS

Two fundamentally different approaches to feature identification, aggregation and boundary approximation for onboard data editing have been examined. Relatively small

differences in accuracies between the simplest boundary approximation and the comparatively complex aggregation method were found, whereas the difference in computational requirements is very large. Further investigation should be performed to determine improvements in feature identification accuracy that may be achieved by careful selection of both the number and location of spectral channels.

The results obtained using the computational model were generally consistent with practical experience with Landsat data in terms of sensitivity to changes in haze, sun angle, and to the set of targets defined. The use of this model as a tool in the preliminary design and evaluation phase of remote sensing systems should prove valuable. To improve computational accuracy it will be necessary to account for the probability of occurence of various targets and the probability of encountering specific atmospheric conditions.

REFERENCES

1. Huck, F. O.; Davis, R. E.; Park, S. K.; Aherron, R. M.; Arduini, R. F.: Computatational Modeling for the Study of Multispectral Sensor Systems and Concepts, Optical Engineering, in press, 1981.
2. Malila, W. A.; Crane, R. B.; Omarzu, C. A.; and Turner, R. E.: Studies of Spectral Discrimination. NASA CR-134181, WRL 31650-22-T, May 1971.
3. Turner, R. E.: Atmospheric Effects in Remote Sensing. Remote Sensing of Earth Resources. ed. F. Shahrokhi, 26-28 March 1973.
4. Turner, R. E.: Atmospheric Effects in Multispectral Remote Sensor Data. NASA CR-ERIM 109600-15-F, May 1975.
5. Kondratyev, K. Ya; Beliavsky, A. I.; and Pokrovsky, O. M.: Possibilities of Optimal Planning of Multipurpose Survey from Space. Proc. of the Thirteenth International Symposium on Remote Sensing of Environment, Environmental Research Institute of Michigan, 32-27 April 1979.
6. Landgrebe, D. A.; Biehl, L. L.; and Simmons, W. R.: An Empirical Study of Scanner System Parameters. IEEE Transactions on Geoscience Electronics, Vol. GE-15, No. 3, July 1977.
7. Wiersma, D. J.;and Landgrebe, D. A.: An Analytical Approach to the Design of Spectral Measurements in the Design of Multispectral Sensor. IEEE Machine Processing of Remoetly Sensed Data Symposium, 1979.
8. Salomonson, V. V.: Landsat D, A Systems Overview. Proc. of the Twelfth Inter-National Symposium on Remote Sensing of the Environment, Vol. II, Environmental Research Institute of Michigan, 20-26 April 1978.
9. Valovcin, F. R.: Spectral Radiance of Snow and Clouds in the Near Infrared Spectral Region. AFGL-TR-78-0289, Air Force Surveys in Geophysics, No. 403, November 17, 1978.
10. Stebbins, W. J.: Snow/Cloud Discrimination Staring Mode Radiometer. Electro-Optics/Laser Conference and Exposition, Boston, Sept. 19-21, 1978.
11. Selby, J. E. A.; Kneizys, F. X.; Chetwynd, J. H., Jr.; and McClatchey, R. A.: Atmospheric Transmittance/Radiance: Computer Code LOWTRAN 4. AFGL-TR-78-0053, Environmental Research Papers, No. 626, Feb. 28, 1978.
12. Maxwell, E. L.: Multivariate System Analysis of Multispectral Imagery. Photogrammetric Engineering and Remote Sensing, Vol. 42, No. 9, Sept. 1976.
13. Duda, R. O.; and Hart, P. E.: Pattern Classification and Scene Analysis. John Wiley and Sons, New York, 1973.
14. Benz, H. F.; Kelly, W. L; Husson, C.; Culotta, P. W.; and Synder, W. E.: CCD Data Processor for Maximum Likelihood Feature Classification, Proc. of the AIAA Sensor Systems for the 80's Conference, Colorado Springs, Dec. 2-4, 1980.

Table 1. Targets and the Assumed Standard Deviation of Their Reflectance

Category	Substance	Standard deviation of reflectance, σ_ρ
I. Vegetation	Barley	.1
	Wheat	.1
	Oats	.1
	Corn	.1
	Aspen	.1
	Red pine	.1
	White pine	.1
II. Bare land	Chernozem-type soil, Nebraska	.125
	Pedialier-type silt, Arkansas	.105
	Pedocal-type soil, Ohio	.105
	Pedocal-type soil, Nebraska	.02
	Quartz sand, Oregon	.140
	Clay, Missouri	.055
	Red quartz and calcite sand, Utah	.105
	Pedocal-type soil, Oklahoma	.09
	Concrete road	.1
	Asphalt road	.1
III. Water	Sea water	.06
IV. Cloud/Snow	Optically thick cloud	.1
	Sugar consistency snow	.08

Table 2. Attenuator Amounts in Vertical Column of Atmosphere

Attenuator	Average value, $\bar{x}$			Standard deviation, σ		
	LOWTRAN	atm·cm	# m^{-2}	LOWTRAN	atm·cm	# m^{-2}
Air (N_2, O_2)	8.0 km	8.0×10^{5}	2.2×10^{29}	0.24 km	2.4×10^{4}	6.5×10^{27}
Aerosol: 23 km visual range	1.5 km	1.5×10^{5}	4.0×10^{28}	0.5 km	0.5×10^{4}	1.4×10^{28}
10 km visual range	3.0 km	3.0×10^{5}	8.1×10^{28}	1.0 km	1.0×10^{5}	2.7×10^{28}
5 km visual range	5.0 km	5.0×10^{5}	1.4×10^{29}	1.7 km	1.7×10^{5}	4.6×10^{28}
Ozone (O_3)	0.34 atm·cm	3.4×10^{-1}	9.2×10^{22}	0.10 atm·cm	1.0×10^{-1}	2.7×10^{22}
Water vapor (H_2O)	1.14 g/cm^2	1.14	3.1×10^{23}	0.36 g/cm^2	3.6×10^{-1}	9.7×10^{22}
Molecular oxygen (O_2)	1.7 km	1.7×10^{5}	4.7×10^{28}	0.12 km	1.2×10^{4}	3.2×10^{27}

Table 3. Computational Requirements for 2 Spectral Channels

Decision Process	Add/Multiplies with number of targets:	
	17	20
MLH	187	220
MSD	68	80
BAM	4	4

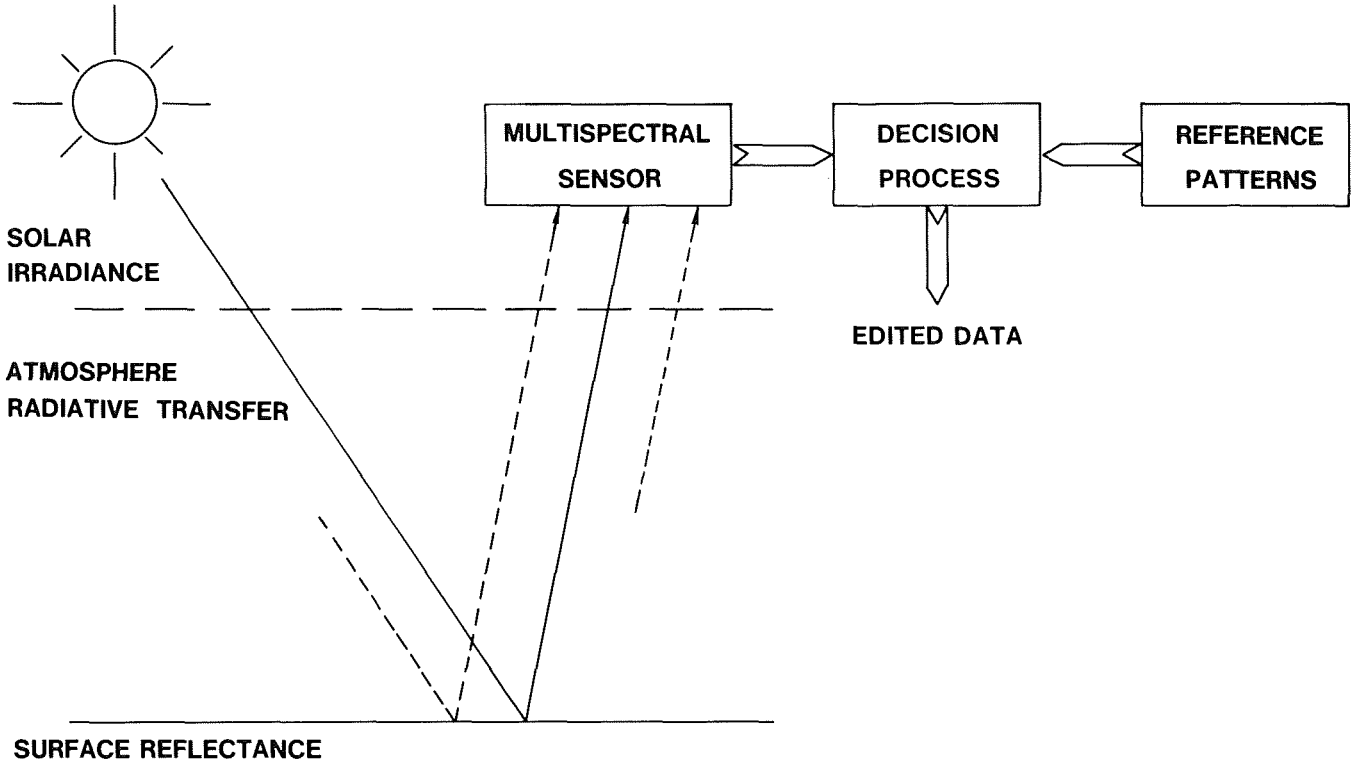

Figure 1.- Data acquisition and decision process.

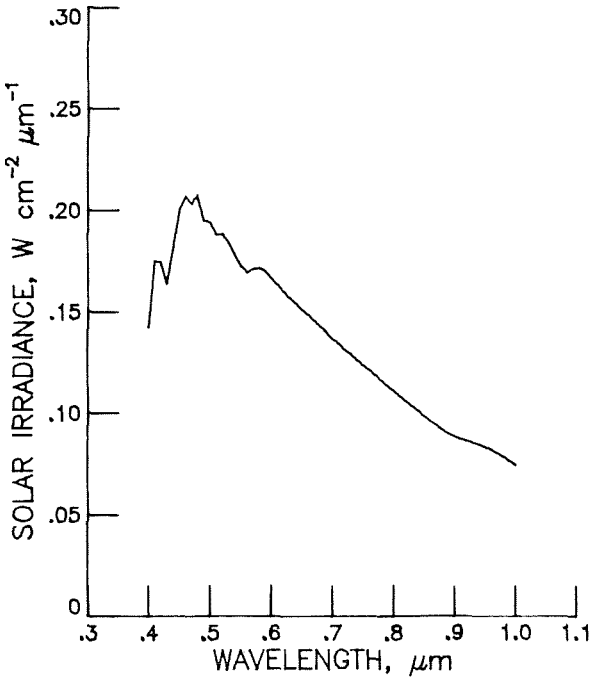

Figure 2.- Solar irradiance at the top of atmosphere.

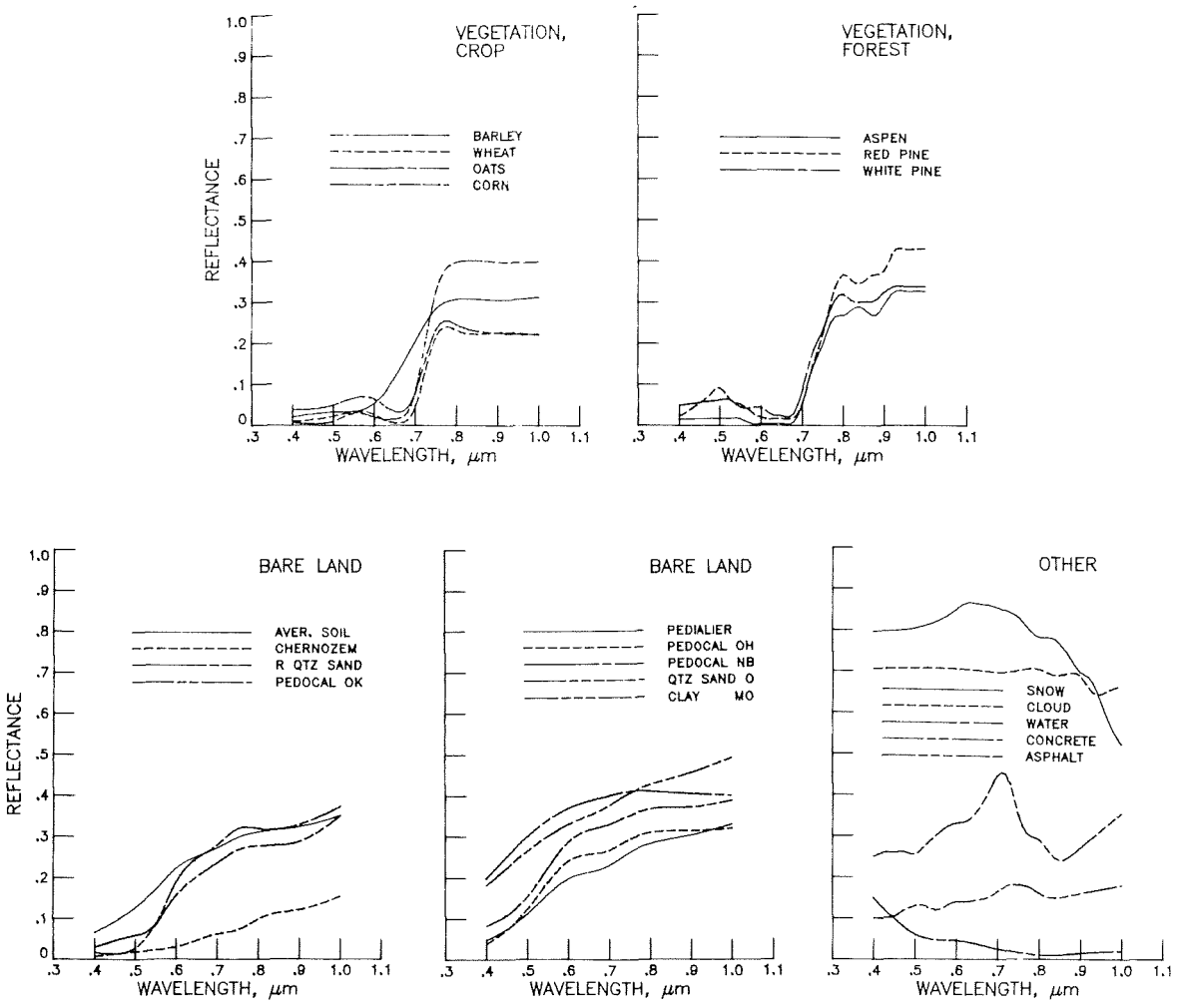

Figure 3.- Spectral reflectances. (See Table 1 for standard deviation of reflectances.)

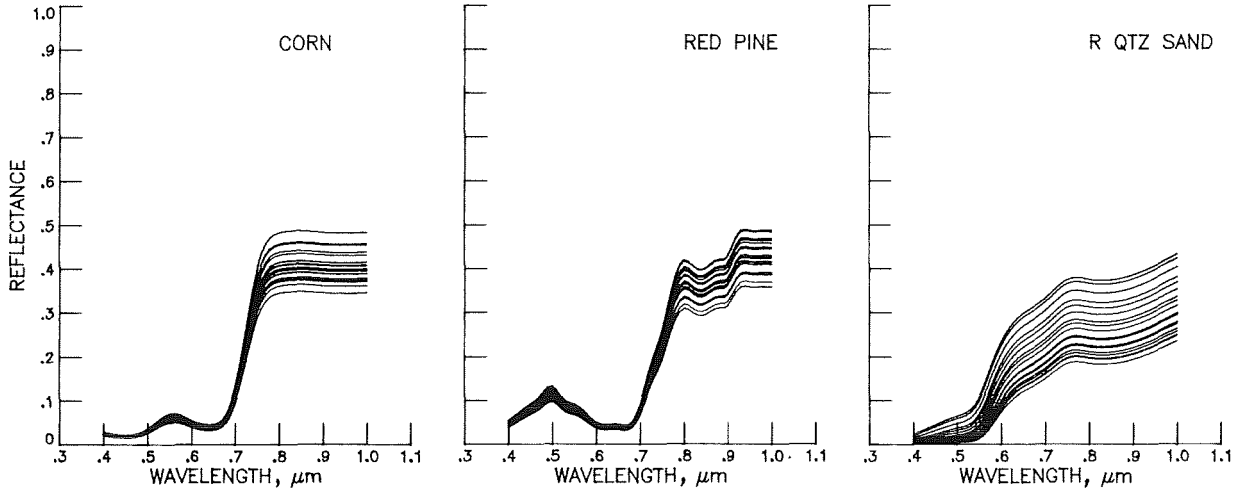

Figure 4.- Typical realization of simulated variability of three spectral reflectances.

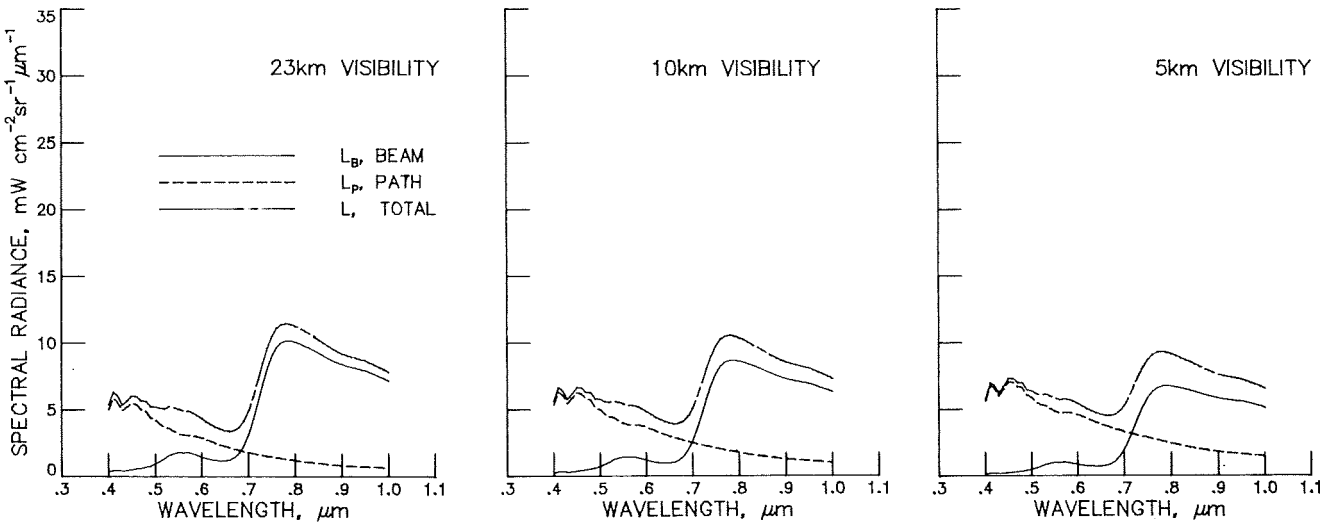

Figure 5.- Average beam, path, and total radiance for corn as target and average soil as background using ERIM radiative transfer model. Exitance is vertical and solar incident angle is 30°.

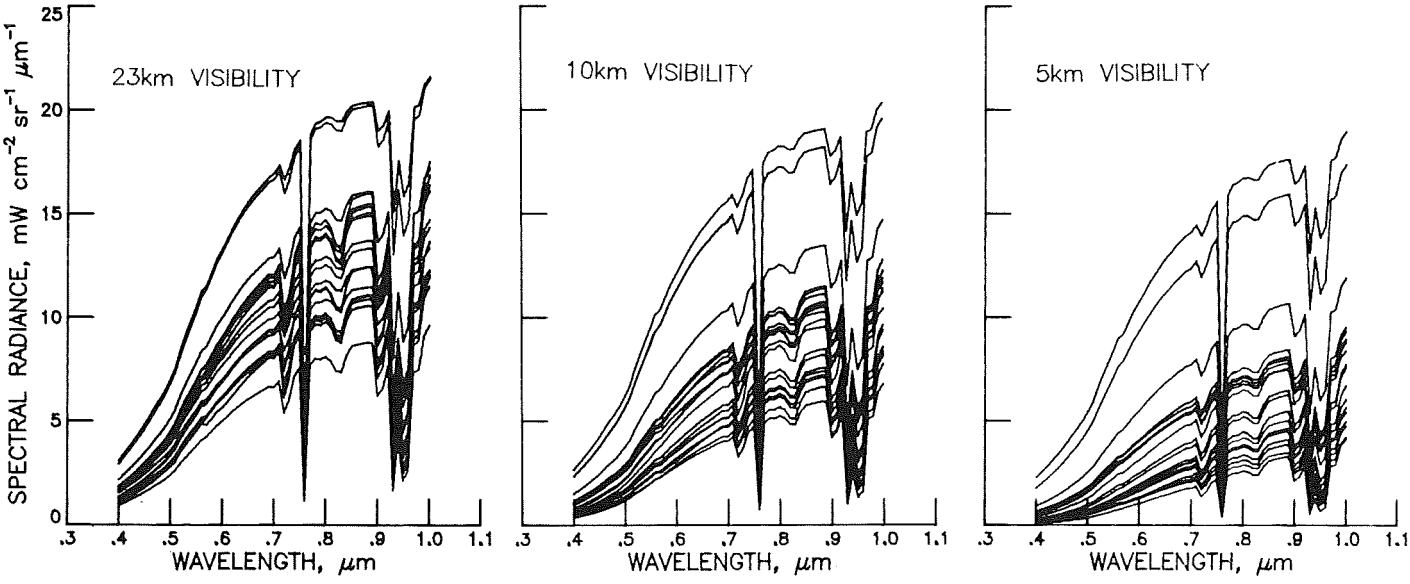

Figure 6.- Typical realization of simulated variability of spectral radiances incident on the multispectral sensor for three visual ranges using LOWTRAN 4. Target is quartz sand and solar incident angle is 30°.

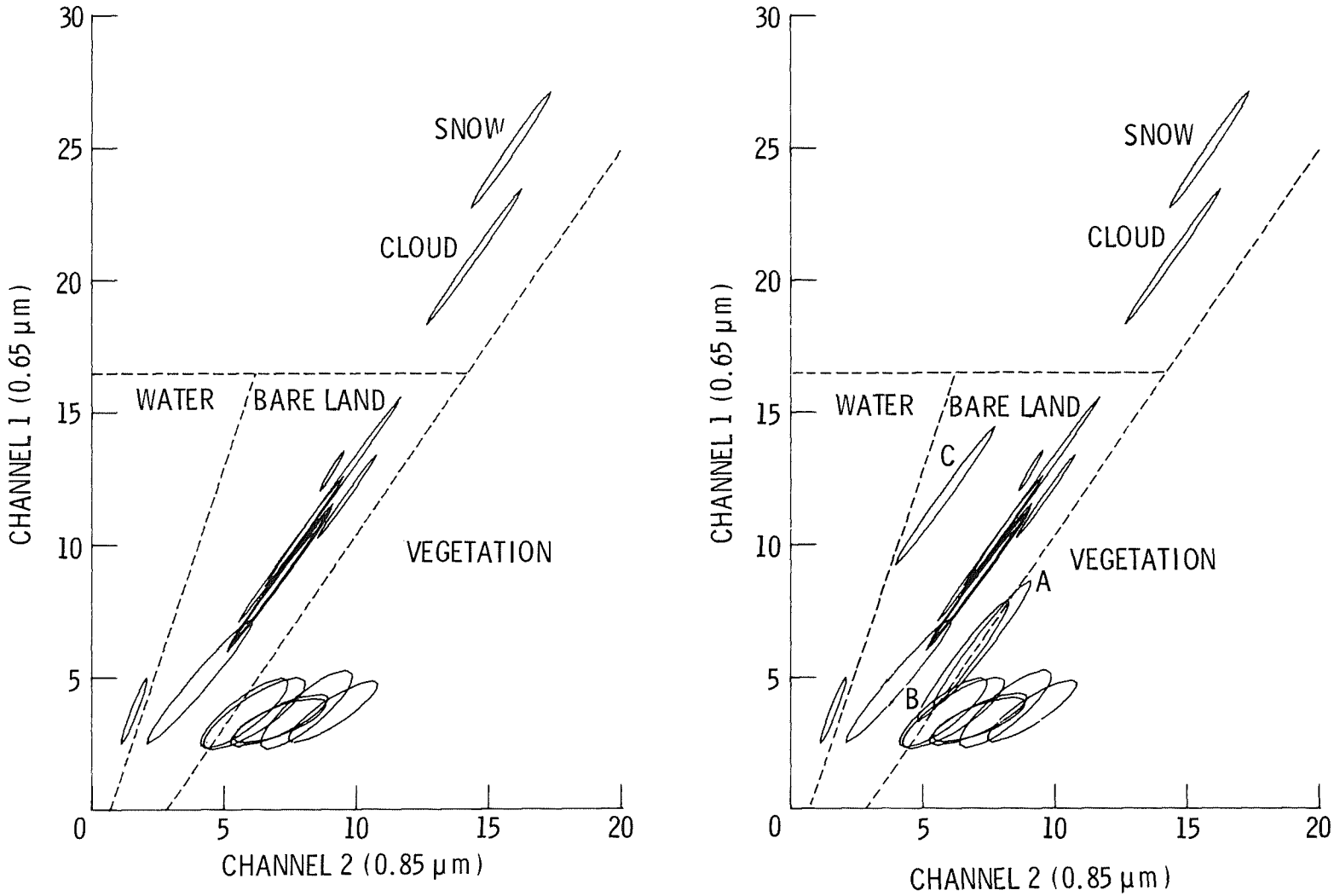

(a) Number of targets is 17; barley, asphalt and concrete are excluded.

(b) Number of targets is 20; barley(B), asphalt (A) and concrete (C) are included.

Figure 7.- Covariance plot of signal from two spectral channels for 23 km visual range and 30° solar incidence angle, and regions used for the boundary approximation method (BAM) decision process.

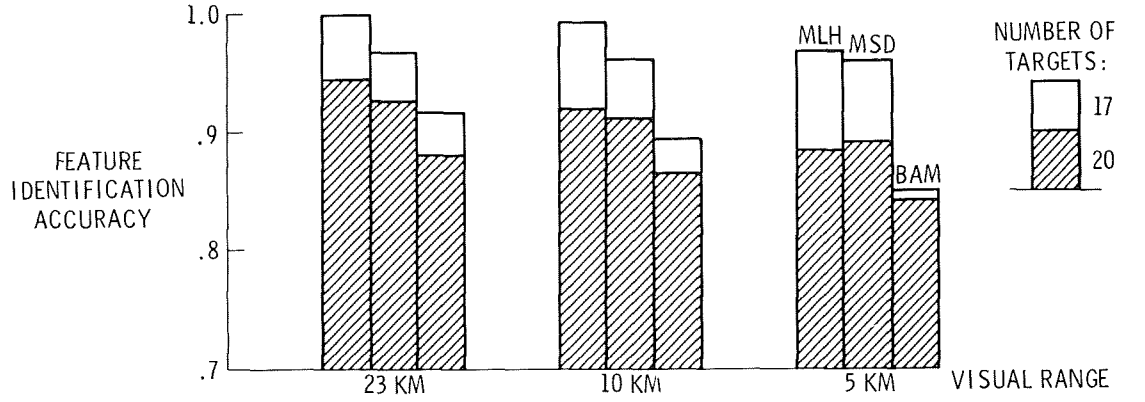

(a) Number of targets is 17 or 20, and data is acquired at a solar incidence angle (SIA) of 30^0.

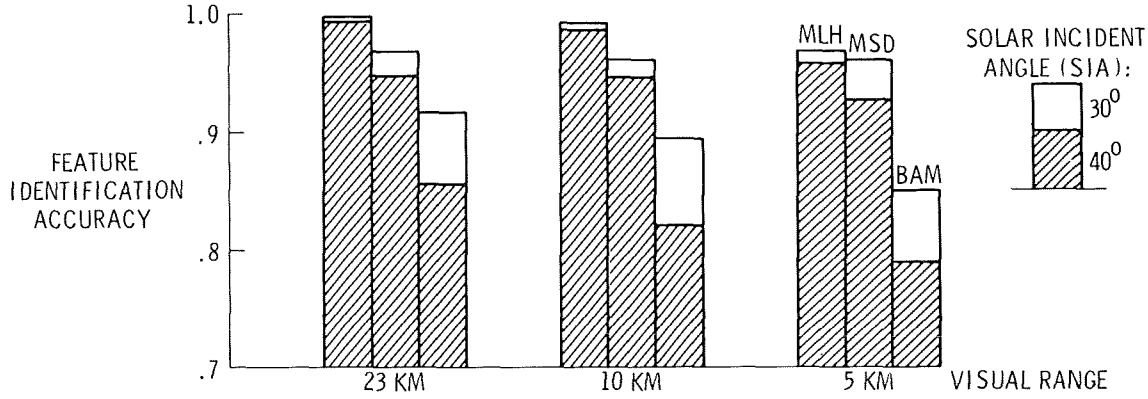

(b) Number of targets is 17, and data is acquired at a SIA of 30^0 or 40^0.

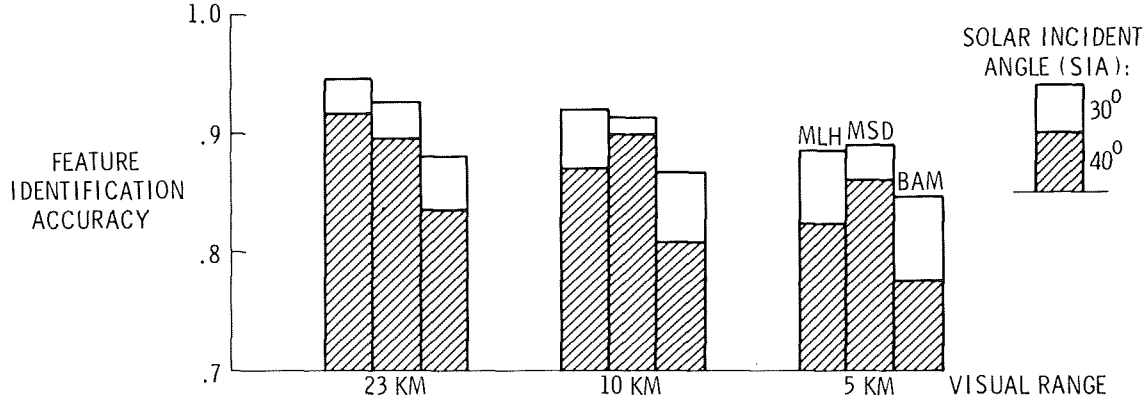

(c) Number of targets is 20, and data is acquired at a SIA of 30^0 or 40^0.

Figure 8.- Feature identification accuracies attained with three decision processes: maximum likelihood (MLH) and mean-square distance (MSD) aggregation method and boundary approximation method (BAM).